PERGAMON

International Journal of Solids and Structures 37 (2000) 1639–1658

INTERNATIONAL JOURNAL OF SOLIDS and STRUCTURES

www.elsevier.com/locate/ijsolstr

# Dynamic fundamental solutions for transversely isotropic piezoelectric materials of crystal class 6 mm

C.H. Daros*, H. Antes

*Institute of Applied Mechanics, Technical University of Braunschweig, Spielmannstr. 11, D-38106 Braunschweig, Germany*

Received 21 July 1998; in revised form 12 October 1998

**Abstract**

In the present work, a fundamental solution for transient 3D dynamic piezoelectricity is derived. The theoretical basics are reviewed with special attention to the case of transversely isotropic piezoelectric materials of the crystal class 6 mm. Numerical results concerning both convex and non-convex slowness surfaces are presented, where different singularities, present only in anisotropic materials, are analysed. 

*Keywords:* Fundamental solutions; Transversely isotropic; Piezoelectric materials

## 1. Introduction

Piezoelectric materials (PEM) have been used in many engineering fields and applications. Perhaps, the most widely spread traditional application of piezoelectric continua is the generation of ultrasonic waves. In the last few years, PEM have also been increasingly applied in the active vibration control of so-called 'smart structures'.

As a consequence of such applications with resulting complex devices, resort must be made to numerical methods. The Boundary Element Method (BEM) has a successful history as a numerical tool to treat dynamic problems as well as local problems such as defects or concentrated loads.

Due to BEM's special qualities, several authors have dedicated their attention to the derivation of fundamental solutions (the basis of BEM) for the case of piezoelectricity. Notwithstanding, such solutions are mathematically difficult to model as PEM have two qualities: anisotropy and electro-mechanical coupling.

Within the framework of time dependent 3D fundamental solutions for PEM there are basically two

* Corresponding author. Fax: 0049 531 391 5843.
*E-mail address:* cd@guzzi.infam.bau.tu-bs.de (C.H. Daros)

0020-7683/00/$ - see front matter 
PII: S0020-7683(98)00308-4

works published in the recent years: the formulation presented in Norris (1994) and the one from Khutoryansky and Sosa (1995a, b). The paper from Norris contains a valuable review on the subject of fundamental solutions for anisotropic solids.

The approach from Khutoryansky and Sosa is based on the representation of the solution over the unit sphere. Moreover, their results went further as the solution was reduced to alternative integrals over a surface (slowness surface) and line integrals.

The idea of representing the fundamental solution over such a surface for the case of aelotropic elastodynamics goes back to Burridge (1967). Actually, this integral formulation over the slowness surface is known as the Hergloz–Petrowski formula. The books of John (1955) and Gelfand and Shilov (1964) give a good description of the ideas that lead to these formulas. By using the slowness surfaces, a great deal of simplification can be achieved, namely the possibility of a line integral representation (Duff, 1977).

The Hergloz–Petrowski formulas are, as noted by Payton (1983), specially suitable in analysing the displacement near the wave front, i.e., the singularities of the fundamental solution. The aforementioned formulas give an explicit expression for the singular part, with no need of any integration.

Contrary to isotropic materials, anisotropy poses a number of difficulties due to the increasing number of singularities of different types. Therefore, it is not surprising that available results for general anisotropy are until now not available. According to Duff (1960) the number of wave fronts in a particular direction in the most anisotropic medium can be as high as 75. This number is even higher when piezoelectricity is present since the slowness surface is raised in degree. For the quasi-electrostatic piezoelectric case, the slowness surface is of degree 8, resulting at most 196 wave fronts (see Salmon, 1927; Duff, 1960).

The results obtained from Burridge and the corresponding generalization for PEM can be theoretically applied to any degree of anisotropy. The implementation is, however, rather cumbersome due to the resulting complexity of the slowness surfaces. On the other hand, few exact surfaces can be found in the literature on particular piezoelectric materials (Dieulesaint and Royer, 1980). For materials with arbitrary piezoelectricity, numerical calculations are necessary. A computational method for determining the slowness surfaces can be found in Strashilov and Gentchev (1987).

The aim of this article is to investigate the potentialities of the Hergloz–Petrowski formulas (with use of a line integral representation) for the case of transversely isotropic piezoelectric materials. The presented numerical results concern both convex and non-convex slowness surfaces, where non-convex slowness surfaces imply a number of interesting physical phenomena as cusps and conical points on the wave surface, resulting in different types of wave front singularities.

## 2. Mathematical preliminaries

Three-dimensional piezoelectricity is governed by a set of four partial differential equations coupling the displacement **u** and the electric potential $\phi$:

$$C_{ijkl}u_{k,lj} + e_{kij}\phi_{,kj} + f_i = \rho\ddot{u}_i$$

$$e_{ikl}u_{k,li} - \varepsilon_{ik}\phi_{,ki} = q \tag{1}$$

where $C_{ijkl}$, $e_{ijk}$ and $\varepsilon_{ij}$ denote the elastic, piezoelectric and dielectric material constants, respectively. **f**, $\rho$ and $q$ stand for the body force per unit of volume, the mass density and the electric charge. Repeated indices are dummy indices (1 to 3 for lower case and 1 to 4 for upper case).

A detailed derivation of the fundamental solution outlined here for eqn (1) can be found in

Khutoryansky and Sosa (1995a, b). At first, an unbounded piezoelectric solid is subjected to two independent states of an impulsive unitary load applied at the source point $\xi$, i.e.,

$$\begin{cases} \mathbf{f} = \delta(t)\delta(\mathbf{x}-\xi)e_j \\ q = 0 \end{cases} \quad \begin{cases} \mathbf{f} = 0 \\ q = -\delta(t)\delta(\mathbf{x}-\xi) \end{cases} \tag{2}$$

with $e_j$ specifying the direction of the applied force. For $\xi = 0$, the loading of eqn (2) yields for eqn (1) the following differential equation,

$$\mathbf{L}(\nabla, \partial_t)\mathbf{U}(\mathbf{x}, t) = \delta(t)\delta(\mathbf{x})\mathbf{I} \tag{3}$$

where $\mathbf{L}(\nabla, \partial_t)$ represents the differential operator,

$$\mathbf{L}(\nabla, \partial_t) = \begin{Vmatrix} \rho\partial_t^2 & 0 \\ 0 & 0 \end{Vmatrix} - \begin{Vmatrix} \mathbf{A} & \mathbf{a} \\ \mathbf{a}^T & -\alpha \end{Vmatrix} \tag{4}$$

with $A_{ik} = C_{ijkl}\partial/\partial x_j\partial/\partial x_l$, $a_i = e_{kij}\partial/\partial x_k\partial/\partial x_j$ and $\alpha = \varepsilon_{ik}\partial/\partial x_i\partial/\partial x_k$. $U$ stands for the $4 \times 4$ symmetric Green's tensor with the following structure

$$\mathbf{U} = \begin{Vmatrix} U_{ij} & U_{i4} \\ U_{4j} & U_{44} \end{Vmatrix}. \tag{5}$$

$U_{ij}$ and $U_{4j}$ are the displacement (in the $i$-direction) and electric potential, respectively, at the observer point $\mathbf{x}$ due to an impulsive force applied at $\xi$ in the $j$ direction. While $U_{i4}$ and $U_{44}$ represent the displacement (in the $i$-direction) and electric potential, respectively, for a point charge applied at $\xi$.

The plane wave transform is now used, where $\delta(x)$ and $\mathbf{U}(\mathbf{x}, t)$ are represented in terms of integrals over the unit sphere $|\mathbf{n}| = 1$ as,

$$\mathbf{U}(\mathbf{x}, t) = \int_{|\mathbf{n}|=1} \mathbf{V}(\mathbf{n}, w, t)\, d\Omega(\mathbf{n}) \quad \delta(x) = -\frac{1}{8\pi^2}\nabla^2 \int_{|\mathbf{n}|=1} \delta(w)\, d\Omega(\mathbf{n}) \quad w = \mathbf{n}\cdot\mathbf{x}. \tag{6}$$

A column of the transformed tensor $\mathbf{V}(\mathbf{n}, w, t)$ can be represented as a four-dimensional column vector $[\mathbf{v}, \phi]$. Substituting eqn (6) into eqn (3) and reducing the resulting coupled system of partial differential equations in $\mathbf{v}$ and $\phi$ to a differential equation in $\mathbf{v}$, one obtains

$$\rho\ddot{\mathbf{v}} - B\mathbf{v}'' = -\frac{1}{8\pi^2}\delta(t)\delta''(w)\mathbf{F} \tag{7}$$

where $\mathbf{B}(\mathbf{n}) = \mathbf{A} + (\mathbf{a}\otimes\mathbf{a})/\alpha$, $\mathbf{F}(\mathbf{n}) = \mathbf{i}_M + \mathbf{a}/\alpha\delta_{4M}$ and $\mathbf{i}_M = [\delta_{1M}, \delta_{2M}, \delta_{3M}]$. Using Duhamel's principle one can rewrite eqn (7) for $t > 0$ as

$$\rho\ddot{\mathbf{v}} - B\mathbf{v}'' = 0 \tag{8}$$

with the initial conditions,

$$\mathbf{v}(\mathbf{n}, w, 0) = 0 \quad \dot{\mathbf{v}}(\mathbf{n}, w, 0) = -\frac{1}{8\pi^2\rho}\delta''(w)\mathbf{F}(\mathbf{n}). \tag{9}$$

Substituting a trial solution in the form of a plane wave $\mathbf{v} = \mathbf{A}g(\mathbf{n}\cdot\mathbf{x} - \lambda t)$, with polarization $\mathbf{A}$ and phase velocity $\lambda$, in eqn (8) results in

$$\mathbf{N}(\mathbf{n}, \lambda)\mathbf{A} = \mathbf{0} \tag{10}$$

with $\mathbf{N}(\mathbf{n}, \lambda) = [\rho\lambda^2\mathbf{1} - \mathbf{B}]$. Eqn (10) shows that the polarization $\mathbf{A}$ is an eigenvector of the tensor $\mathbf{B}(\mathbf{n})$ with the eigenvalue $\gamma = \rho\lambda^2$. As noted by Khutoryansky and Sosa (1995a), the tensor $\mathbf{B}$ is bounded, symmetric and positive definite. Moreover, its three eigenvalues are real positive numbers, upper and lower bounded with respect to $\mathbf{n}$. $\lambda_i = \sqrt{\gamma_i/\rho}$, $\lambda_{3+i} = -\lambda_i$ are the real roots of the characteristic equation (also known as the secular equation) $\det \mathbf{N}(\mathbf{n}, \lambda) = 0$. Furthermore, the three eigenvectors $\mathbf{A}^{(i)}$ corresponding to the eigenvalues $\gamma_i$ form an orthonormal set

$$\sum_{i=1}^{3} \mathbf{A}^{(i)}(\mathbf{n}) \otimes \mathbf{A}^{(i)}(\mathbf{n}_0) = \mathbf{I}$$

since the tensor $\mathbf{B}(\mathbf{n})$ is symmetric.

A solution of eqn (8) with the initial conditions (9) can be derived by making use of the first term in eqn (6) and assuming some results present in Khutoryansky and Sosa (1995a) like

$$\mathbf{U}_{iM}(\mathbf{x}, t) = -\frac{H(t)}{4\pi^2}\frac{\partial}{\partial t}\int_{|n|=1} \sum_{i=1}^{3} \delta(y)\, \mathrm{res}\left\{\lambda^{-2} N_{\mathrm{ij}}^{-1}(\mathbf{n}, \lambda)\right\}_{\lambda=\lambda_{\mathrm{i}}} \mathrm{F}_{\mathrm{jM}}(\mathbf{n})\, \mathrm{d}\Omega(\mathbf{n}) \tag{11}$$

$$U_{4M}(\mathbf{x}, t) = -\frac{H(t)}{4\pi^2}\frac{\partial}{\partial t}\int_{|n|=1} \sum_{i=1}^{3} \delta(y)\, \mathrm{res}\left\{\lambda^{-2} N_{\mathrm{ij}}^{-1}(\mathbf{n}, \lambda)\right\}_{\lambda=\lambda_{\mathrm{i}}} \mathbf{F}_{\mathrm{jM}}(\mathbf{n})\frac{\mathbf{a}_i(\mathbf{n})}{\alpha(\mathbf{n})}\, \mathrm{d}\Omega(\mathbf{n}) - \frac{\delta(t)\delta_{4M}}{4\pi\sqrt{\varepsilon_{ij}^c x_i x_k}} \tag{12}$$

where $y = t - \mathbf{x}\cdot\mathbf{n}/\lambda_i$ and $\varepsilon_{ik}^c$ are the cofactors of the dielectric tensor $\varepsilon_{ij}$. It is also important to note that the above summation is valid over distinct roots $\lambda_i$ only (non-repeated eigenvalues). The three real positive roots, that are present in eqns (11) and (12), represent the velocities of three plane waves propagating in the same direction with different velocities. The polarizations of the three plane waves are always mutually orthogonal since $\mathbf{B}$ is symmetric. The displacement vector $\mathbf{v}$ is generally not parallel or perpendicular to $\mathbf{n}$. Therefore, there are in most of the cases two quasi-transverse ($qT$) waves and one quasi-longitudinal ($qL$) wave (which is the fastest one). Making use of

$$\sum_{i=1}^{3} \mathrm{res}\left\{\lambda \mathbf{N}_{\mathrm{ij}}^{-1}(\mathbf{n}, \lambda)\right\}_{\lambda=\lambda_i} = \mathbf{1}/\rho$$

and some symmetries (which allow to write the results in terms of the positive $\lambda_i$) one obtains for eqn (11) a similar expression to that of Burridge (1967),

$$U_{iM}(\mathbf{x}, t) = -\frac{H(t)}{8\pi^2\rho}\sum_{i=1}^{3}\int_{|n|=1} \frac{\mathbf{A}^{(i)}(\mathbf{n}) \otimes \mathbf{A}^{(i)}(\mathbf{n})}{\lambda_i(\mathbf{n})}\delta'\big(\lambda_i(\mathbf{n})t - \mathbf{n}\cdot\mathbf{x}\big)\mathbf{F}(\mathbf{n})\, \mathrm{d}\Omega(\mathbf{n}) \tag{13}$$

where $\delta'(\lambda_i(\mathbf{n})t - \mathbf{n}\cdot\mathbf{x}) = \lambda_i^{-2}\partial\delta(y)/\partial t$ for $\lambda_i > 0$. The factor $\Lambda_{ij}^{(i)} = A_i^{(i)}A_j^{(i)}$ (see Every and Kim, 1994), to be seen as the weighting for each plane wave contributing to $U_{ij}(\mathbf{x}, t)$, depends on the projection of the polarization vector of that wave on the sensing and forcing directions.

The fundamental solution presented in eqns (11) and (12) can be transduced into an alternative form, which is computationally more attractive. Using the concept of the slowness surfaces, the 2D integrals can be reduced to a simple line integral.

The slowness surface for a certain material is determined by a vector $\mathbf{s} = \mathbf{n}/\lambda_i(\mathbf{n})$, which has the same direction of the normal vector $\mathbf{n}$ but the inverse magnitude of the phase velocity $\lambda$ of a plane wave moving in the $n$-direction. A representation of this surface can be achieved by using the secular equation

and noting that $\det \mathbf{N}(\mathbf{n}, \lambda) = \lambda^6 \det \mathbf{N}(\mathbf{s}, 1)$; one can express the surface as

$$Q(\mathbf{s}) = \det \mathbf{N}(\mathbf{s}, 1) = 0. \tag{14}$$

For anisotropic materials, this surface is composed of three distinct sheets (see Fig. 2) whereas for isotropic materials two sheets coincide. In order to write the fundamental solution in terms of the slowness surface, the following coordinate system transformation is used

$$\mathrm{d}\boldsymbol{\Omega}(\mathbf{n}) = \frac{|\mathbf{s}\cdot\nabla\mathbf{Q}|}{|\mathbf{s}|^3|\nabla\mathbf{Q}|}\,\mathrm{d}S(\mathbf{s}) \tag{15}$$

where $\mathrm{d}S(\mathbf{s})$ is the element of area of the slowness surface. Using eqn (15), expressions (11) and (12) result in

$$\mathbf{U}_{iM}(\mathbf{x}, t) = \frac{H(t)}{4\pi^2}\frac{\partial}{\partial t}\int_{Q=0}\frac{\operatorname{sgn}(\mathbf{s}\cdot\nabla\mathbf{Q})}{|\nabla\mathbf{Q}|}\mathbf{P}_{ij}(\mathbf{s})\mathbf{F}_{jM}\delta(t-\mathbf{x}\cdot\mathbf{s})\,\mathrm{d}S(\mathbf{s}) \tag{16}$$

$$\mathbf{U}_{4M}(\mathbf{x}, t) = \frac{H(t)}{4\pi^2}\frac{\partial}{\partial t}\int_{Q=0}\frac{\operatorname{sgn}(\mathbf{s}\cdot\nabla\mathbf{Q})}{\alpha(\mathbf{s})|\nabla\mathbf{Q}|}\mathbf{P}_{ij}(\mathbf{s})\mathbf{F}_{jM}a_i(\mathbf{s})\delta(t-\mathbf{x}\cdot\mathbf{s})\,\mathrm{d}S(\mathbf{s}) - \frac{\delta(t)\delta_{4M}}{4\pi\sqrt{\varepsilon^c_{ik}x_i x_k}} \tag{17}$$

where $\mathbf{P}(\mathbf{s}) = \mathbf{N}^a(\mathbf{s}, 1)$ (adjoint matrix of $\mathbf{N}$) and sgn is the signum function. The only $s$-space points which contribute to the surface integrations in eqns (16) and (17) are those formed from the intersection of the slowness surface and the plane $t = \mathbf{x}\cdot\mathbf{s}$ moving in the $\mathbf{x}$-direction. This locus of intersection points is here represented by the line $l(\mathbf{x}, t)$ (see Fig. 2). After some mathematical manipulations, one obtains the final representation for the fundamental solution like

$$\mathbf{U}_{iM}(\mathbf{x}, t) = \frac{H(t)}{4\pi^2}\frac{\partial}{\partial t}\int_{l(\mathbf{x},\,t)}\mathbf{M}^{**}_{iM}(\mathbf{s})\,\mathrm{d}l(\mathbf{s}) \tag{18}$$

$$\mathbf{U}_{4M}(\mathbf{x}, t) = \frac{H(t)}{4\pi^2}\frac{\partial}{\partial t}\int_{l(\mathbf{x},\,t)}\frac{\mathbf{M}^{**}_{iM}(\mathbf{s})a_i(\mathbf{s})}{\alpha(\mathbf{s})}\,\mathrm{d}l(\mathbf{s}) - \frac{\delta(t)\delta_{4M}}{4\pi\sqrt{\varepsilon^c_{ik}x_i x_k}} \tag{19}$$

with

$$\mathbf{M}^{**}_{iM}(\mathbf{s}) = \frac{\operatorname{sgn}(\mathbf{s}\cdot\nabla\mathbf{Q})\mathbf{P}_{ij}(\mathbf{s})\mathbf{F}_{jM}}{\sqrt{|\mathbf{x}|^2|\nabla\mathbf{Q}|^2 - (\mathbf{x}\cdot\nabla\mathbf{Q})^2}}. \tag{20}$$

One advantageous characteristic of eqns (18) and (19) is that the delta distribution does not appear in the fundamental solution. Moreover, when the vector $\nabla Q(\mathbf{s})$ (whose direction is normal to the slowness surface) for $\mathbf{s} \in l(\mathbf{x}, t)$ is parallel to $\mathbf{x}$, the fundamental solution presents a singularity (for details, see Section 5). It is also important to observe that for double points, i.e., when two sheets of the slowness surface meet (mathematically $\{Q(\mathbf{s}) = 0, \nabla Q(\mathbf{s}) = 0\}$), the integrands in eqns (18) and (19) become indeterminate. For double points present at the analysed transversely isotropic materials (the poles of the two most external slowness sheets) a simple L'Hospital rule can be applied to remove the indetermination $\mathbf{M}^{**}_{iM}(\mathbf{s}) = 0/0$.

## 3. The Green's tensor for the crystal class 6 mm

The previous results are now specialized for a special class of transversely isotropic piezoelectric materials, namely the class 6 mm. This is an important piezo-material class, since it includes, e.g., poled piezoceramics like $BaTiO_3$, PZT-4, PZT-6*B*, and other piezocrystals like ZnO.

The adjoint matrix $\mathbf{N}^a(\mathbf{n}, \lambda)$ and the operator $Q = \det \mathbf{N}(\mathbf{n}, \lambda)$, which compose the inverse matrix $\mathbf{N}^{-1}(\mathbf{n}, \lambda) = \mathbf{N}^a(\mathbf{n}, \lambda)/\det \mathbf{N}(\mathbf{n}, \lambda)$ in eqn (11), can be written for the class 6 mm like

$$\mathbf{N}^a = \begin{vmatrix} D + n_1^2 G & n_1 n_2 G & -EJ n_1 n_3 \\ n_1 n_2 G & D + n_2^2 G & -EJ n_2 n_3 \\ -EJ n_1 n_3 & -EJ n_2 n_3 & EK \end{vmatrix} \tag{21}$$

with the operators $G$, $J$, $K$ and $Q$,

$$\begin{aligned} G(n_1, n_2, n_3, \lambda) = {} & \left[ (c_{13} + c_{44})^2 - \frac{1}{2}(c_{11} + c_{12}) c_{33} \right. \\ & \left. + \frac{2(c_{13} + c_{44})(e_{15} + e_{31}) e_p - (e_{15} + e_{31})^2 c_{33} n_3^2}{\varepsilon\varepsilon} \right] n_3^2 \\ & - \left[ \frac{1}{2}(c_{11} + c_{12}) c_{44} + \frac{(e_{15} + e_{31})^2 c_{44} n_3^2}{\varepsilon\varepsilon} \right] \left(n_1^2 + n_2^2\right) - \frac{1}{2} \frac{(c_{11} + c_{12}) e_p^2}{\varepsilon\varepsilon} \\ & + \left[ \frac{1}{2}(c_{11} + c_{12}) + \frac{(e_{15} + e_{31})^2 n_3^2}{\varepsilon\varepsilon} \right] \rho\lambda^2 \end{aligned} \tag{22}$$

$$J(n_1, n_2, n_3) = (c_{13} + c_{44}) + (e_{15} + e_{31}) \frac{e_p}{\varepsilon\varepsilon} \tag{23}$$

$$K(n_1, n_2, n_3, \lambda) = c_{44} n_3^2 + \left[ c_{11} + \frac{(e_{15} + e_{31})^2 n_3^2}{\varepsilon\varepsilon} \right] \left(n_1^2 + n_2^2\right) - \rho\lambda^2 \tag{24}$$

$$\begin{aligned} Q(n_1, n_2, n_3, \lambda) = ED = {} & - \left[ c_{44} n_3^2 + \frac{1}{2}(c_{11} - c_{12}) \left(n_1^2 + n_2^2\right) - \rho\lambda^2 \right] \left[ c_{44} c_{33} n_3^4 \right. \\ & + \left\{ c_{44}^2 + c_{11} c_{33} - (c_{13} + c_{44})^2 \right\} n_3^2 \left(n_1^2 + n_2^2\right) + c_{44} c_{11} \left(n_1^2 + n_2^2\right)^2 \\ & + \left( c_{44} \left(n_1^2 + n_2^2\right) + c_{33} n_3^2 \right) \frac{(e_{15} + e_{31})^2 \left(n_1^2 + n_2^2\right) n_3^2}{\varepsilon\varepsilon} \\ & - 2(c_{13} + c_{44})(e_{15} + e_{31}) \frac{e_p \left(n_1^2 + n_2^2\right) n_3^2}{\varepsilon\varepsilon} + \left( c_{44} n_3^2 + c_{11} \left(n_1^2 + n_2^2\right) \right) \frac{e_p^2}{\varepsilon\varepsilon} \\ & \left. - \left\{ (c_{33} + c_{44}) n_3^2 + (c_{11} + c_{44}) \left(n_1^2 + n_2^2\right) \right\} \rho\lambda^2 - \frac{(e_{15} + e_{31})^2 \left(n_1^2 + n_2^2\right) n_3^2 + e_p^2}{\varepsilon\varepsilon} \rho\lambda^2 + \rho^2 \lambda^4 \right] \end{aligned} \tag{25}$$

with $e_p = e_{15}(n_1^2 + n_2^2) + e_{33} n_3^2$ and $\varepsilon\varepsilon = \varepsilon_{11}(n_1^2 + n_2^2) + \varepsilon_{33} n_3^2$. The operator $Q(\mathbf{n}, \lambda)$ can be factored like in the case of transversely isotropy Payton (1983) into a product of a second degree operator $E$ and a

fourth degree operator $D(\mathbf{n}, -V) = A_p(\mathbf{n}) - V^2 B_p(\mathbf{n}) + V^4$ in $V$. Where $V = \rho^{1/2}\lambda$ and $A_p(\mathbf{n})$, $B_p(\mathbf{n})$ can easily be obtained from eqn (25).

Now, similar to Payton's analysis (see Payton, 1983), it holds

$$\operatorname{sgn}(-\mathbf{s}\cdot\nabla\mathbf{D}) = -4A_pR^4 + 2B_pR^2 = 2A_p\left(\frac{1}{A_p} - R^4\right) \tag{26}$$

resulting $\operatorname{sgn}(-\mathbf{s}\cdot\nabla\mathbf{D}) = +1$ on $S_I$ and $\operatorname{sgn}(-\mathbf{s}\cdot\nabla\mathbf{D}) = -1$ on $S_{II}$, where $s_1^2 + s_2^2 = R^2\sin^2\theta$, $s_3^2 = R^2\cos^2\theta$ and $R(\theta)$ satisfying $D(\mathbf{s}, -1) = 0$. Hence, the elastodynamic tensor for the class 6 mm may be written as

$$U_{11}(x,y,z,t) = -\frac{H(t)}{4\pi^2}\frac{\partial}{\partial t}\int_{Q=0}\frac{\operatorname{sgn}(\mathbf{s}\cdot\nabla\mathbf{Q})\big(D(\mathbf{s}) + s_1^2 G(\mathbf{s})\big)}{|\nabla\mathbf{Q}|}\delta(t - \mathbf{x}\cdot\mathbf{s})\,\mathrm{d}S(\mathbf{s}) \tag{27}$$

$$U_{12}(x,y,z,t) = -\frac{H(t)}{4\pi^2}\frac{\partial}{\partial t}\int_{Q=0}\frac{\operatorname{sgn}(\mathbf{s}\cdot\nabla\mathbf{Q})s_1s_2G(\mathbf{s})}{|\nabla\mathbf{Q}|}\delta(t - \mathbf{x}\cdot\mathbf{s})\,\mathrm{d}S(\mathbf{s}) \tag{28}$$

$$U_{13}(x,y,z,t) = -\frac{H(t)}{4\pi^2}\frac{\partial}{\partial t}\int_{S_I}\frac{s_1s_3J(\mathbf{s_I})}{|\nabla\mathbf{D}|}\delta(t - \mathbf{x}\cdot\mathbf{s_I})\,\mathrm{d}S_I + \frac{H(t)}{4\pi^2}\frac{\partial}{\partial t}\int_{S_{II}}\frac{s_1s_3J(\mathbf{s_{II}})}{|\nabla\mathbf{D}|}\delta(t - \mathbf{x}\cdot\mathbf{s_{II}})\,\mathrm{d}S_{II} \tag{29}$$

$$U_{33}(x,y,z,t) = \frac{H(t)}{4\pi^2}\frac{\partial}{\partial t}\int_{S_I}\frac{K(\mathbf{s_I})}{|\nabla\mathbf{D}|}\delta(t - \mathbf{x}\cdot\mathbf{s_I})\,\mathrm{d}S_I - \frac{H(t)}{4\pi^2}\frac{\partial}{\partial t}\int_{S_{II}}\frac{K(\mathbf{s_{II}})}{|\nabla\mathbf{D}|}\delta(t - \mathbf{x}\cdot\mathbf{s_{II}})\,\mathrm{d}S_{II}. \tag{30}$$

The above four components are sufficient to represent the tensor $U_{ii}$ since the following symmetries $U_{21}(x,y,z,t) = U_{12}(x,y,z,t)$, $U_{22}(x,y,z,t) = U_{11}(y,x,z,t)$, $U_{23}(x,y,z,t) = U_{13}(y,x,z,t)$ and $U_{32}(x,y,z,t) = U_{23}(x,y,z,t)$ are valid for hexagonal materials.

## 4. Characteristic surfaces

Three characteristic surfaces are used to analyse the elastic wave propagation in anisotropic solids. Each surface in turn is composed of three distinct sheets.

The first surface is the velocity surface, which is traced out as the normal $\mathbf{n}$ in the vector $\mathbf{v} = \lambda\mathbf{n}$ with the amplitude of the phase velocity $\lambda$, takes all possible plane wave propagation directions. This surface has generally one quasi-longitudinal sheet ($qL$) and 2 quasi-transversal sheets ($qT$). Usually, the $qL$ sheet contains both $qT$ sheets as the $qL$ waves are faster than the other two.

The second surface is the already defined slowness surface. The $qL$ sheet, which now is the innermost one, is always convex (Duff, 1960) when the piezoelectric coupling is absent.

On the other hand, when piezoelectricity exists, the innermost sheet $qL$ may present concavities. This fact was illustrated by Every and McCurdy (1987) and Every and Neiman (1992). Considering piezoelectric solids and a quasi-electrostatic approximation, the slowness surface is now of degree 8 instead of 6 when piezoelectricity is absent. Rochelle salt (orthorhombic, crystal class 222) and $Ba_2NaNb_5O_{15}$ (class mm 2) are two examples of piezoelectric materials with non-convex innermost slowness surfaces.

As a result of a possible non-convexity of the innermost sheet of the slowness surface, the $qL$ mode can give rise to caustics (i.e., temporal singularities).

The last surface is known as the wave front surface. The latter contains a front of three sheets emitted

by a point source at the origin and at time $t = 0$. According to the wave construction method of Huyghens (see Payton, 1983), the general form of the wave front surface at a subsequent time $t$ is given by the envelope of plane fronts which passed through the origin at $t = 0$. The reader is referred to Musgrave (1970) for a complete description of these surfaces.

The slowness surface furnishes a powerful projective relationship to the wave front surface, which influences the form of the singularities of the fundamental solution. Therefore, some projective correspondences between the slowness $S$ and wave surfaces $W$ will be presented. The case here illustrated shows typical features found on transversely isotropic materials. For such materials, one of the sheets corresponds to a pure transversely polarized mode, $T$. This sheet, which is not affected by the piezoelectric coupling, is convex, whereas the remaining $qT$ and $qL$ sheets can be non-convex. Furthermore, the characteristic surfaces are obtained by rotating the symmetry plane $x_1$, $x_3$ around the symmetry axis $x_3$.

The points at the slowness surface are classified as elliptic, parabolic or hyperbolic depending on the principal curvatures $l$ and $n$ of the slowness surface (Payton, 1983). Points $Q_\infty$ in $S$ with a common tangent plane $P^\infty$ (in [0, 0, 1]) map onto a conical point $p^\infty$ in $W$ on the $\xi_3$ axis. Parabolic points $Q$ correspond to cusp points $p$ in $W$. Finally, points like $Q_{II}$ with common tangent plane $P^{II}$ give rise to double points $p_{II}$ in $W$.

## 5. Singularities of the fundamental solution

An important contribution to the understanding of the propagation mechanism of elastic waves in an anisotropic medium (and consequently the singularities of the fundamental solution) owes to Duff (1960). He made use of the slowness and the wave surfaces to obtain a solution for the Cauchy problem, considering the general theory of hyperbolic differential equations. In his work, Duff describes the solution as a sum of a sharp wave, on each sheet of the wave surface, and a continuous wave in the regions between the outer and innermost wave surface. The innermost region of the wave front surface is a 'lacuna' (or gap) and there is no propagation of waves behind the last sheet of the wave surface, confirming the Huyghens Principle (i.e., the clean cut wave propagation in one or three space dimensions). So, the fundamental solution will always terminate with a sharp wave. The continuous wave, on the other hand, can arrive before the first sharp wave when the outermost sheet of the wave surface is non-convex.

Duff (1977) and Burridge (1967) have obtained asymptotic results of the Herglotz–Petrowski formula valid near the wavefront for anisotropic elastic waves. Duff (1977) analysed the asymptotic behaviour of the Herglotz–Petrowski formulas for higher order hyperbolic equations, revealing the straightforward relation between the slowness and wave front surfaces. Using expressions similar to eqns (16) and (17), Duff describes that, as $t$ increases, the plane $t = \mathbf{x} \cdot \mathbf{s}$ moves away from the origin and an instant $t'$, at which it is tangent to a slowness sheet $S_i$, is the moment at which the corresponding wave sheet $W_i$ reaches the point $\mathbf{x}$. As $t \to t'$, the intersection of the variable plane with $S$ shrinks to a point and disappears. Thus, the singularity on a sheet $W_i$ (except for the case of a conical point in $W_i$) is contributed by a small patch of $S_i$ where $\mathbf{n}$, the outward normal to the sheet $S_i$, is parallel to $\mathbf{x}$.

Following the ideas from Duff (1960), Burridge (1967) and later Khutoryansky and Sosa (1995b) have separated the singular and regular (in time) parts of the fundamental solution:

$$\mathbf{U}(\mathbf{x}, t) = \mathbf{U}^{\delta}(\mathbf{x}, t) + \mathbf{U}^{R}(\mathbf{x}, t), \tag{31}$$

where the term $\mathbf{U}^R$ is a continuous function bounded in time. So, the singularities or jumps in the

solution are described exclusively by the first term in eqn (31) that represents the sharp waves on $W$ or the corresponding asymptotic Herglotz–Petrowski formulas on $S$.

The singularities on the wave front surface can have different forms depending on the classification of the corresponding point (or points) on the slowness surface and whether the point lies on a symmetry direction or not.

In view of the numerical examples, the presented singularities refer to a concentrated point force with Heaviside step function dependence rather than a Dirac Delta one (which can be achieved simply deriving the presented results with respect to time). A detailed description of the following singularities, which may occur in the case of transversely isotropic materials, can be found in Payton (1983), Burridge (1967) and Every and Kim (1994).

### 5.1. Elliptic points on the slowness surface

When both principal curvatures $l$ and $n$ are of the same sign, the slowness surface is elliptic meaning that it is either convex or concave. Supposing that the vanishing cycle on $S_i$ corresponding to the space vector $x$ has coordinates $s_1, s_2, s_3$ with origin at a point $\mathbf{s}_0$ on the slowness sheet. Moreover, considering the $s_3$ axis parallel to $x$ and letting the $s_1$ and $s_2$ axes be along lines of principal curvature at $\mathbf{s}_0$, the equation for the area $S_i$ surrounding $\mathbf{s}_0$ can be assumed as

$$s_3 = -\alpha s_1^2 - \beta s_2^2 \tag{32}$$

where $\alpha = l/2$ and $\beta = n/2$. The element of area is $\mathrm{d}S = \mathrm{d}s_1\,\mathrm{d}s_2$. Then, on $S$, $\mathbf{x}\cdot\mathbf{s} = \mathbf{x}\cdot\mathbf{s}_0 + |\mathbf{x}|s_3 = \mathbf{x}\cdot\mathbf{s}_0 - \alpha s_1^2 - \beta s_2^2$. The singular part of eqn (16), for example, derives from an integral of the form

$$\mathbf{U}^{\delta}_{iM}(\mathbf{x}, t)|_{\mathbf{s}_0} \sim -\int \mathbf{M}(\mathbf{s})\delta\big(T + \big[\alpha s_1^2 + \beta s_2^2\big]|\mathbf{x}|\big)\,\mathrm{d}s_1\,\mathrm{d}s_2 \tag{33}$$

where $T = t - \mathbf{x}\cdot\mathbf{s}_0$ and $\mathbf{M}(\mathbf{s}) = (\mathrm{sgn}(\mathbf{s}\cdot\nabla\mathbf{Q})\mathbf{P}_{ij}(\mathbf{s})\mathbf{F}_{jM}(\mathbf{s}))/(4\pi^2|\nabla\mathbf{Q}|)$. The integration of the form present in eqn (33) has been evaluated (Payton, 1983; Every and Kim, 1994) resulting in

$$\mathbf{U}^{\delta}_{iM}(\mathbf{x}, t)|_{\mathbf{s}_0} \sim -\frac{\mathbf{M}(\mathbf{s}_0)\pi}{\sqrt{\alpha\beta}|\mathbf{x}|}H[\mp T] \tag{34}$$

where the argument in the Heaviside function is $-T$ for $\alpha, \beta > 0$ and $+T$ for $\alpha, \beta < 0$. The term $K = 4\alpha\beta$ is known as the Gaussian curvature of the slowness surface and is invariant with respect to axes of reference. As it can be seen, the discontinuity is a far-field effect decaying with the distance from the source like $|x|^{-1}$.

### 5.2. Hyperbolic points on the slowness surface

If one of the principal curvatures, e.g., $l$ is negative and the other one is positive, the slowness surface is saddle-shaped at $\mathbf{s}_0$ and called hyperbolic. Following Payton (1983) or Every and Kim (1994) at that point, near $T = 0$, the solution presents a logarithmic divergence like

$$\mathbf{U}^{\delta}_{iM}(\mathbf{x}, t)|_{s_0} \sim \frac{\mathbf{M}(\mathbf{s}_0)}{\sqrt{-\alpha\beta}|\mathbf{x}|}\ln[|T|]. \tag{35}$$

### 5.3. Parabolic points on the slowness surface

Parabolic points on the slowness surface correspond to points where the Gaussian curvature is zero. These points map onto cuspidal edges (folds) in the wave surface. As noted by Every and Kim (1994) (see Fig. 1), on the inside of the fold there are two closely spaced wave fronts corresponding to points $\mathbf{s}_a$ and $\mathbf{s}_b$ on either side of the parabolic line where the slowness surface is saddle-shaped and convex (or concave). As the fold is approached, the Gaussian curvature at $\mathbf{s}_a$ and $\mathbf{s}_b$ tends to zero and the magnitude of the discontinuity and logarithmic divergence increase as they progressively get closer in time. At the cuspidal edge, these coalesce and give rise to a higher order singularity. Supposing $n = 0$ and $l > 0$, the approximation for the slowness surface must be carried to cubic terms in $s_2$ so that $s_3 = -(\alpha s_1^2 + \gamma s_2^3) + \cdots$, with $\gamma$ positive. Following a similar procedure to that outlined in eqn (33), one obtains the divergence

$$\mathbf{U}_{iM}^{\delta}(\mathbf{x}, t)|_{\mathbf{s}_0} \sim -\frac{\mathbf{M}(\mathbf{s}_0) g\big(\mathrm{sgn}(T)\big)}{\alpha^{1/2}\gamma^{1/3}|\mathbf{x}|^{5/6}|T|^{1/6}}, \tag{36}$$

where $g(+) = 2.429$ and $g(-) = 4.206$. Eqn (36) represents a $1/|T|^{1/6}$ divergence falling off with a $1/|\mathbf{x}|^{5/6}$ dependence on the distance.

### 5.4. Conical point in the wave surface

As already seen in Fig. 1, the wave surface of transversely isotropic solids may have a conical point along the principal symmetry axis. Then, the tangent plane $t = \mathbf{x} \cdot \mathbf{s}$ touches the $qT$ slowness sheet along a closed curve. The behaviour of the singularity at the conical point can be found in (Payton, 1983) as

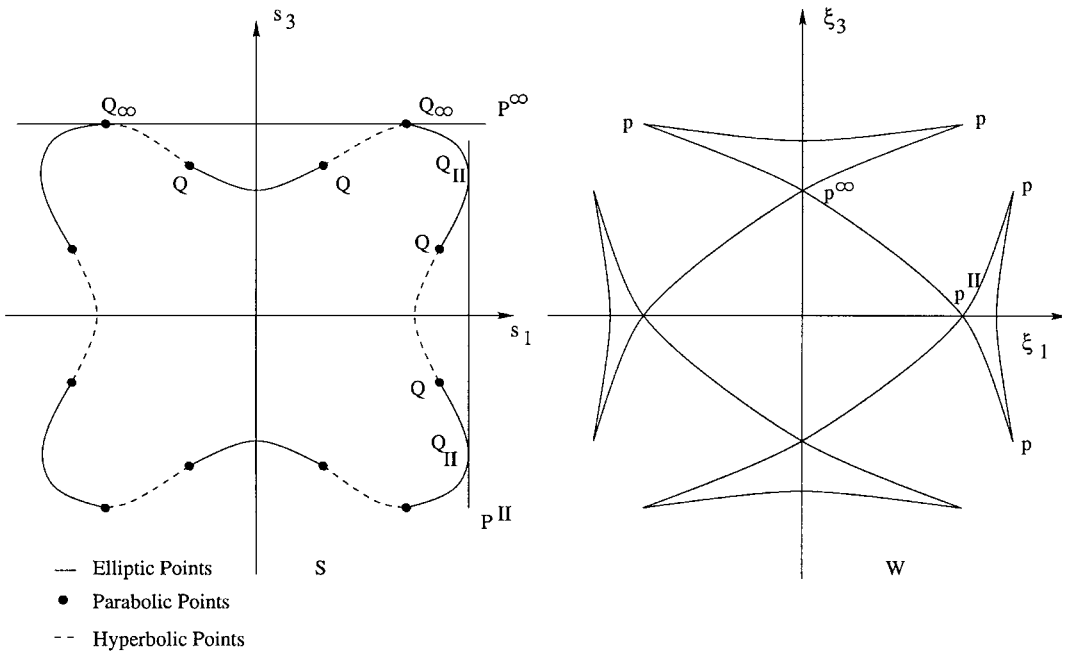


Fig. 1. Slowness and wave curves of a transversely isotropic solid.

$$\mathbf{U}^{\delta}_{iM}(\mathbf{x}, t)|_{\mathbf{s}_0} \sim 1/\sqrt{|T||\mathbf{x}|}, \quad T < 0 \tag{37}$$

$$\mathbf{U}^{\delta}_{iM}(\mathbf{x}, t)|_{\mathbf{s}_0} \sim 1/|\mathbf{x}|, \quad T > 0. \tag{38}$$

### 5.5. Lower order singularities

Lower order singularities of the fundamental solution for anisotropic solids were first observed by Every and Kim (1994). These singularities take place when the forcing or sensing direction is perpendicular to the polarization vector $\mathbf{A}_i(\mathbf{s}_0)$, then $\det|\Lambda_{ij}| = 0$. The case of vanishing $\Lambda_{ij}$ can be found in symmetry planes of the considered medium and the case of transversely isotropic media is a good example of how these singularities arise.

Considering $\mathbf{s}_0$ located in the transverse symmetry plane $x_1, x_3$ with $x_2$ perpendicular to it, one has $\mathbf{U}^{\delta}_{12} = \mathbf{U}^{\delta}_{21} = \mathbf{U}^{\delta}_{32} = \mathbf{U}^{\delta}_{23} = 0$. Moreover, for the pure transverse mode, $\mathbf{A}_i(\mathbf{s}_0) = (0, 1, 0)$ resulting in $\Lambda_{11}(\mathbf{s}_0) = \Lambda_{33}(\mathbf{s}_0) = \Lambda_{13}(\mathbf{s}_0) = \Lambda_{31}(\mathbf{s}_0) = 0$. Then, the $\mathbf{U}^{\delta}_{11}, \mathbf{U}^{\delta}_{33}, \mathbf{U}^{\delta}_{13}, \mathbf{U}^{\delta}_{31}$ elastodynamic components of $\mathbf{U}^{\delta}_{ij}$ present a lower order singularity instead of a discontinuity. Remembering that

$$\sum_{N=1}^{3} \mathbf{A}^N_i(\mathbf{s}_0)\mathbf{A}^N_j(\mathbf{s}_0) = \mathbf{I},$$

the $qL$ and $qT$ modes are now polarized in the symmetry plane meaning that for these modes it is $\Lambda_{22}(\mathbf{s}_0)$ that takes a zero value. The corresponding $\Lambda_{ij}(\mathbf{s})$ zero terms have to be expanded in powers of $s_1$ and $s_2$ (the local coordinate system located at $\mathbf{s}_0$) in order to analyse their lower order singularities.

On planes of symmetry, the weighting factor $\Lambda_{ij}(\mathbf{s})$ can be assumed simply as $\Lambda_{ij}(\mathbf{s}) \approx as_2^2$ (where $a$ is a constant). Then, e.g., using eqn (16), the elastodynamic components for elliptic points can be written as

$$\mathbf{U}^{\delta}_{ij}(\mathbf{x}, t)|_{\mathbf{s}_0} \sim -\mathbf{F}a \int s_2^2 \delta\big(T + \big[\alpha s_1^2 + \beta s_2^2\big]|\mathbf{x}|\big)\, \mathrm{d}s_1\, \mathrm{d}s_2. \tag{39}$$

The above integral has the following evaluation:

$$\mathbf{U}^{\delta}_{ij}(\mathbf{x}, t)|_{\mathbf{s}_0} \sim -\frac{\mathbf{F}a\pi}{2\sqrt{\alpha\beta^3}|\mathbf{x}|^2}|T|H[\mp T] \tag{40}$$

with $-T$ for $\alpha, \beta > 0$ and $+T$ for $\alpha, \beta < 0$. At $T = 0$, $\mathbf{U}^{\delta}_{ij}$ displays a kink and $\mathrm{d}\mathbf{U}^{\delta}_{ij}/\mathrm{d}T$ a discontinuity decreasing as $1/|\mathbf{x}|^2$. A procedure, similar to the one outlined here, can be applied for hyperbolic and parabolic points. For hyperbolic points, the time derivative of $\mathbf{U}^{\delta}_{ij}$ results a $\ln|T|$ divergence whereas for parabolic points a divergence like $1/|T|^{1/6}$ appears.

## 6. Numerical location of $l(\mathbf{x}, t)$

Although the line integral representations in eqns (18) and (19) are formally simple, the line $l(x, t)$ has to be located numerically. Therefore, an efficient numerical method to locate $l(x, t)$ plays a decisive role in determining the fundamental tensor $\mathbf{U}_{MM}(\mathbf{x}, t)$. As it will be seen, a semi-analytical location of $l(x, t)$ is possible for transversely isotropic solids (including the piezoelectric case).

For the aforementioned class of anisotropic solids, the secular equation can be solved resulting for the symmetry plane $x1$, $x3$ (Dieulesaint and Royer, 1980) the three following slowness curves: $S_I$ for the $qL$ mode, $S_{II}$ corresponding to the $qT$ mode and finally $S_{III}$, the not piezoelectrically active pure $T$ mode.

$$S_{I(+),II(-)} = \left( \frac{2\rho}{\Gamma_{22} + \Gamma_{33} \pm \sqrt{(\Gamma_{22} - \Gamma_{33})^2 + 4\Gamma_{23}^2}} \right)^{1/2} \tag{41}$$

$$S_{III} = \sqrt{\rho/\Gamma_{11}} \tag{42}$$

where $\Gamma_{11} = c_{66}n_1^2 + c_{44}n_3^2$, $\Gamma_{22} = c_{11}n_1^2 + c_{44}n_3^2 + \gamma_2^2/\varepsilon$, $\Gamma_{23} = (c_{13} + c_{44})n_1n_3 + (\gamma_2\gamma_3)/\varepsilon$, $\Gamma_{33} = c_{44}n_1^2 + c_{33}n_3^2 + \gamma_3^2/\varepsilon$, with $\gamma_2 = (e_{15} + e_{31})n_1n_3$, $\gamma_3 = e_{15}n_1^2 + e_{33}n_3^2$, $\varepsilon = \varepsilon_{11}n_1^2 + \varepsilon_{33}n_3^2$, and $n_1 = \sin\theta$, $n_3 = \cos\theta$. Rotation of these curves about the $x_3$-axis yields the three sheets of the slowness surface. Obviously, the operators $E$ and $D$, derived in Section 3, can also be used to obtain eqns (41) and (42) (see Payton, 1983).

The line $l(\mathbf{x}, t)$ on a sheet $S_j$ is defined over directions for which $t - \mathbf{s}\cdot\mathbf{x} = 0$. The coordinates $s1$, $s2$, $s3$ of a sheet can be written in terms of spherical coordinates as

$$\mathbf{s}(\theta, \phi) = \big(S_j \sin\theta\cos\phi,\ S_j \sin\theta \sin\phi,\ S_j \cos\theta\big) \tag{43}$$

where $S_j$ is a function of $\theta$ and the symmetry plane is defined by $s1$, $s3$ where $\phi = 0$.

Using eqn (43), a solution in $\phi$ can be found for $t - \mathbf{s}\cdot\mathbf{x} = 0$ like

$$\phi_1 = 2\arctan\big(b/(2a)\big), \quad \phi_2 = 2\arctan\big(c/(2a)\big) \tag{44}$$

with terms $a = -S_jx_1n_1 + S_jx_3n_3 - t$, $b = -2S_jx_2n_1 + 2\sqrt{d}$, $c = -2S_jx_2n_1 - 2\sqrt{d}$, and $d = S_j^2(x_2^2n_1^2$

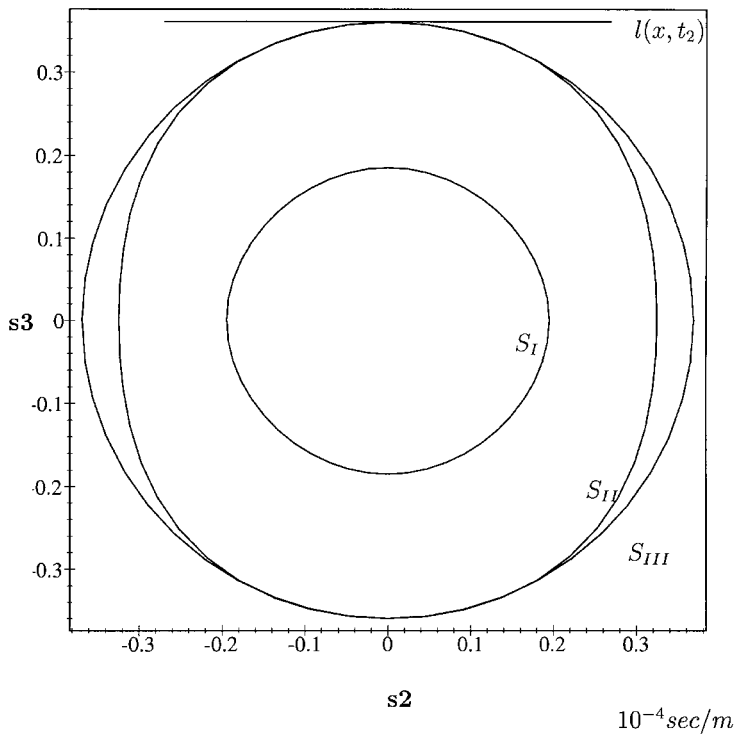


Fig. 2. Slowness sheets for $BaTiO_3$.

$+ x_1^2 n_1^2 - x_3^2 n_3^2) + 2S_j x_3 n_3 t - t^2$. Solutions in eqn (44) depend on the variable $\theta$. The limits of the line $l(x, t)$ in terms of $\theta$ can be found assuming that $\phi_1 = \phi_2$, which in turn means that $d = 0$. The limit values $\theta_{1L}$ and $\theta_{2L}$ (roots of the equation $d = 0$) have to be evaluated numerically, e.g., using a one-dimensional root finding algorithm.

Nevertheless, the $qT$ sheet in the analysed examples can be non-convex, which implies that for a certain time $t$ the line $l(\mathbf{x}, t)$ may be composed of more than a single closed curve. Payton (1983) developed an extensive work classifying transversely isotropic materials according to the shape of the $S_{II}$ curve in the symmetry plane $s1$, $s3$. In view of his five possible classes (which may be applied to the following piezoelectric examples), a straight line intercepts the curve $S_{II}$ at most four times so there are maximum two closed curves that compose $l(\mathbf{x}, t)$. For this case, $d = 0$ presents four different roots $(\theta_1 < \theta_2 < \theta_3 < \theta_4)$ and,

$$l(x, t):[\phi_1, \phi_2](\theta_1 \leqslant \theta \leqslant \theta_2) \bigcup [\phi_1, \phi_2](\theta_3 \leqslant \theta \leqslant \theta_4). \tag{45}$$

On the other hand, considering the operator $D$ of degree 6 in $\mathbf{s}$, a straight line might intercept, e.g., the sheet $S_{II}$ up to six times, rendering then three closed curves for $l(\mathbf{x}, t)$.

## 7. Numerical examples

Making use of the integrated fundamental solution, some results are here presented for transversely isotropic materials including the piezoelectric coupling.

By integrating the fundamental solution with respect to time, one obtains for eqn (18), e.g.,

$$\mathbf{U}_{iM}(\mathbf{x}, t) = \frac{H(t)}{4\pi^2} \int_{l(\mathbf{x},\, t)} M_{iM}^{**}(\mathbf{s})\, \mathrm{d}l(\mathbf{s}) - \frac{H(t)}{4\pi^2} \int_{l_1} M_{iM}^{**}(\mathbf{s})\, \mathrm{d}l(\mathbf{s}) \tag{46}$$

where the second term in eqn (46) states for the static solution of the problem. For $t = 0$, the plane $\mathbf{x} \cdot \mathbf{s} = 0$ is perpendicular to $|\mathbf{x}|$ defining the line $l_1(\mathbf{x}, t = 0)$. The static part of eqn (46) can be also represented using the unit sphere where now $l_1$ is the intersection of the sphere with $\mathbf{x} \cdot \mathbf{n} = 0$ (corresponding to the results of Chen, 1993). More recently, explicit results for the static transversely isotropic case were obtained by Ding et al. (1996), Akamatsu and Tanuma (1997) and Dunn and Wienecke (1996). After the plane containing $l(x, t)$ crosses the last slowness sheet, the first term in eqn (46) vanishes and the displacements remain constant due to the static term. The calculated static values of the numerical examples were checked with the explicit solution from Ding et al. (1996).

Another important feature of the present examples is the causality effect, i.e., $U_{ii}(\mathbf{x}, t) = 0$ for a time '$t$' preceeding the wave front arrival at $\mathbf{x}$.

For the following numerical examples, the $T$ mode is polarized in the [010] direction, while $qL$ and $qT$ are polarized in the symmetry plane.

### 7.1. $BaTiO_3$

The first example is the piezoceramic $BaTiO_3$, which belongs to the class of transversely isotropic materials and whose sheets ($S_I$, $S_{II}$, $S_{II}$) are convex (see Fig. 2). Fig. 3 shows components of the fundamental tensor $\mathbf{U}_{ii}(\mathbf{x}, t)$ when a point force is applied at (0, 0, 0) and the observer is located at the symmetry axis (0, 0, 1). The latter is an acoustic axis, i.e., an axis along which a $T$ wave may propagate with any polarization. The line $l(\mathbf{x}, t)$ reaches $S_I$ at $t_1 \approx 1.8 \times 10^{-4}$ s and $S_{II}$, $S_{III}$ at $t_2 \approx 3.6 \times 10^{-4}$ s. For

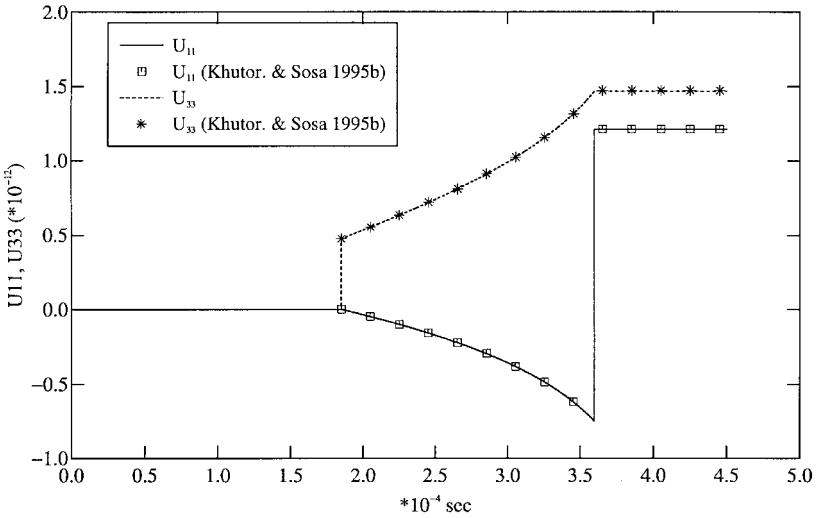


Fig. 3. $U_{11}$ and $U_{33}$ for $BaTiO_3$, $\mathbf{x} = (0, 0, 1)$.

$U_{33}$ in Fig. 3, there is a discontinuity at $t_1(\Lambda = 1)$ corresponding to a pure longitudinal mode polarized at [0, 0, 1] and a kink at $t_2$. For $U_{11} = U_{22}$, there is a kink ($\Lambda = 0$) at $t_1$ and a discontinuity at $t_2$.

For Fig. 4, the observation point is now located at (1, 0, 0). $l(\mathbf{x}, t)$ reaches $S_I, S_{II}$ and $S_{III}$ at $t_1 \approx 2.0 \times 10^{-4}$ s, $t_2 \approx 3.25 \times 10^{-4}$ s, and $t_3 \approx 3.65 \times 10^{-4}$ s, respectively. The pure transverse mode does not contribute to the components $U_{33}$, $U_{31}$, $U_{13}$, $U_{23}$ and $U_{32}$ (e.g., $U_{33}$ in Fig. 4 maintains its value after $t_2$). This becomes evident when specializing the Green's tensor for hexagonal crystals (see eqns (29) and (30)).

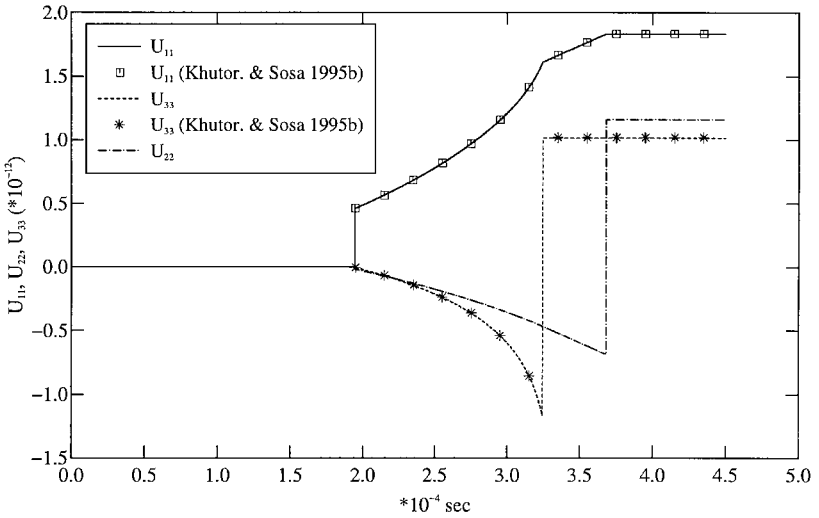


Fig. 4. $U_{11}$, $U_{22}$ and $U_{33}$ for $BaTiO_3$, $\mathbf{x} = (1, 0, 0)$.

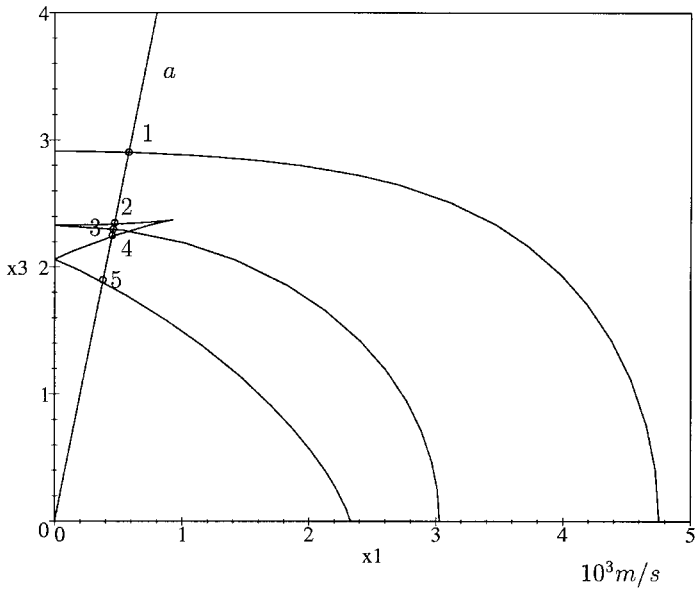


Fig. 5. Cross-section of the wave surface of zinc by the symmetry plane $(x_1, x_3)$.

### 7.2. Zinc

The second example is the hexagonal crystal zinc. The formulas here presented can be used to elastic problems by simply neglecting the piezoelectric coupling. Fig. 5 shows the (010) section of the wave surface of zinc and the propagation direction $a$. The $qT$ slowness sheet is non-convex meaning that its wave sheet is folded. Figs. 6 and 7 show the components $U_{11}$ and $U_{22}$ in the direction $a$. For $U_{11}$, there is a small discontinuity at 1 ($\Lambda \approx 0$), a large discontinuity at 2 ($\Lambda \approx 1$), a kink at 3 ($\Lambda = 0$), a logarithmic

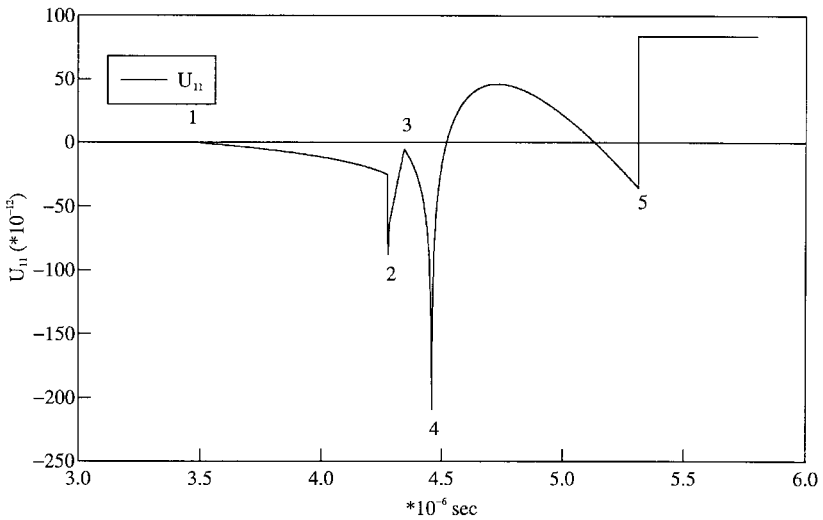


Fig. 6. $U_{11}$ for zinc in direction $a$, $\mathbf{x} = (0.002, 0, 0.01)$.

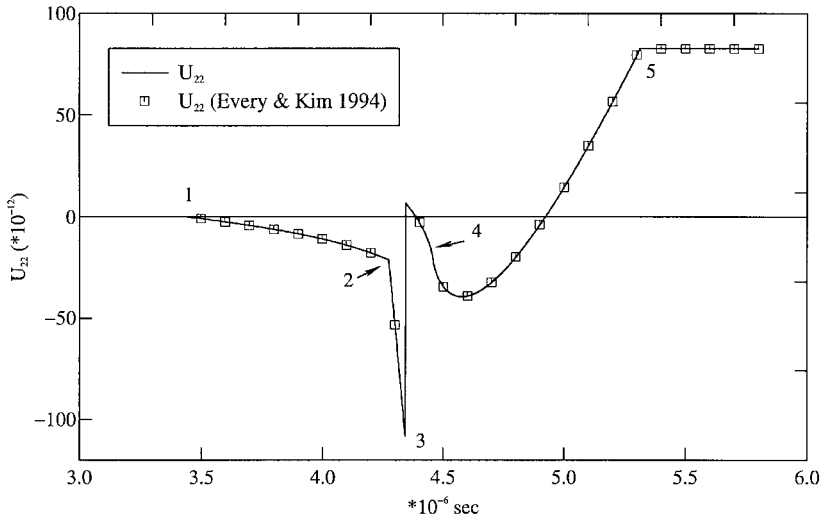


Fig. 7. $U_{22}$ for zinc in direction $a$, $\mathbf{x} = (0.002, 0, 0.01)$.

divergence at 4 and a discontinuity at 5. The results presented in Fig. 7 are compared to the 2D integration over the unit sphere performed by Every and Kim (1994). For a $10^{-9}$ time discretization the computational time for this example is about 20 s on a Power PC.

### 7.3. Zinc oxide

The third example is the hexagonal piezocrystal zinc oxide, which has a non-convex $qT$ slowness sheet like zinc. Fig. 8 shows the (010) section of the wave surface for the material. The analysed direction $b$, $\mathbf{x} = (0.67483, 0, 0.73797)$, includes the cusp point 2. The time values for the points 1, 2, 3, and 4 are $t_1 \approx 1.68 \times 10^{-4}$ s, $t_2 \approx 3.06 \times 10^{-4}$ s, $t_3 \approx 3.21 \times 10^{-4}$ s, and $t_4 \approx 3.62 \times 10^{-4}$ s, respectively. Fig. 9 shows the response functions $U_{11}$ and $U_{33}$ for direction $b$ along the symmetry axis. For $U_{11}$ and $U_{33}$, there is a discontinuity at 1 and 3. At the cusp point 2, $U_{33}$ shows a weak negative divergence ($\Lambda \ll 1$) and $U_{11}$ a large negative divergence ($\Lambda \approx 1$). At point 4, $U_{11}$ shows a kink ($\Lambda = 0$) whereas $U_{33}$ has no singular behaviour for the pure transverse mode. A similar analysis can be used for the response functions presented in Fig. 10. The crosses in Figs. 9 and 10 and points represent hereafter the calculated analytical values of the discontinuities in the fundamental solution.

## 8. Numerical aspects of the implementation

In this section, some aspects of the present numerical implementation are explained in detail. The first step is the exact location of the time discontinuities, which lay on the wave surface. Using the duality of $W$ and $S$, every point $\mathbf{s}$ of $S$ whose normal is parallel to the position vector $\mathbf{x}$ corresponds to a point on $W$. Hence, the time discontinuities are obtained by $t^* = \mathbf{s} \cdot \mathbf{x}$. For a given vector $\mathbf{x}$ with its polar coordinate $\theta_x$, the polar coordinates $\theta_W$ of the points on an hexagonal sheet $S_j$, which correspond to $W_j$, are

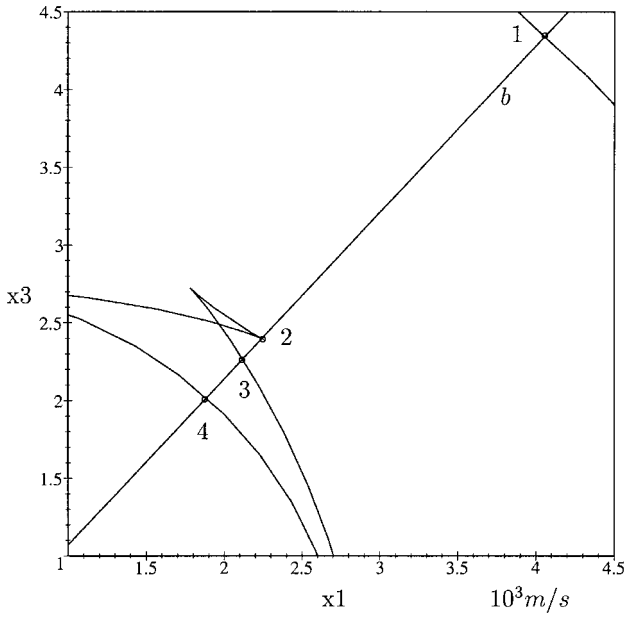


Fig. 8. Cross-section of the wave surface of zinc oxide by a meridian plane.

$$\theta_W = \text{Zeros of}\left\{\cos\theta_x - \frac{S_j\cos\theta + \left(\partial S_j/\partial\theta\right)\sin\theta}{\sqrt{S_j^2 + \left(\partial S_j/\partial\theta\right)^2}}\right\}_{0<\theta<\pi}. \tag{47}$$

With the knowledge of the set of wave fronts $t^*$'s for a certain $\mathbf{x}$, one can restrict the numerical evaluation of the Green's tensor between the first and last wave fronts, but, of course, only when assuming the innermost sheet of $S$ to be convex.

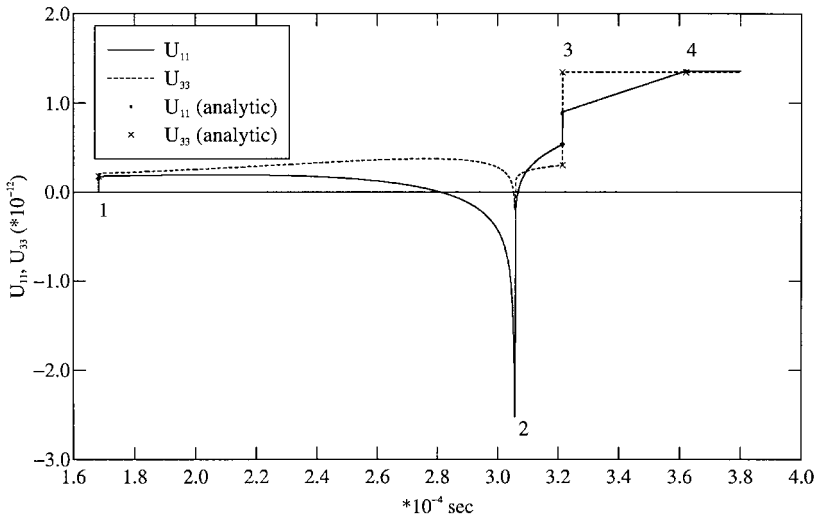


Fig. 9. $U_{11}$ and $U_{33}$ for zinc oxide in direction $b$, $\mathbf{x} = (0.67483, 0, 0.73797)$.

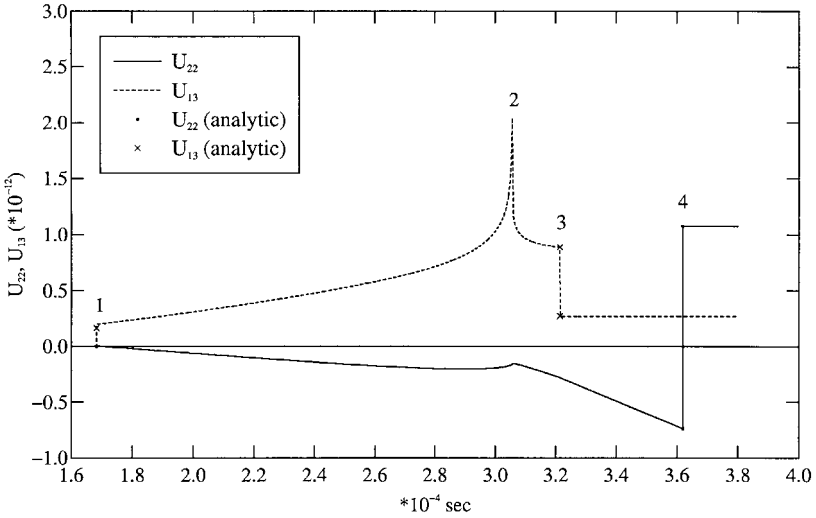


Fig. 10. $U_{13}$ and $U_{22}$ for zinc oxide in direction $b$, $\mathbf{x} = (0.67483, 0, 0.73797)$.

Another point to be examined is the numerical integration of $l(x, t)$. In the present implementation, the semi-analytical location (see eqn (45)) was used, where the kernel $M$ was integrated on $l(\mathbf{x}, t)$ using quadratic elements, hence, using three nodal values for each element. In order to achieve a good accuracy, ten Gauss points were used in the numerical integration. Fig. 11 shows a plane section on the $S_{II}$ sheet of PZT-6$B$, where $l(\mathbf{x}, t)$ is discretized using four quadratic elements.

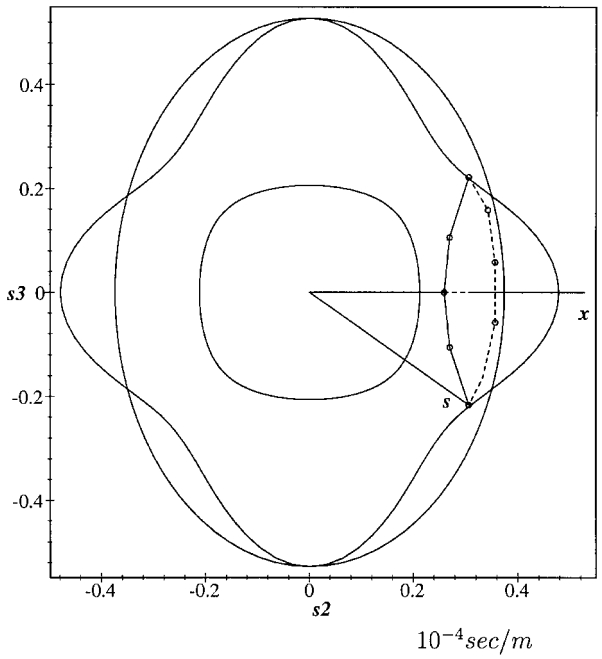


Fig. 11. Slowness sheets for PZT-6$B$ with a plane section on $S_{II}$.

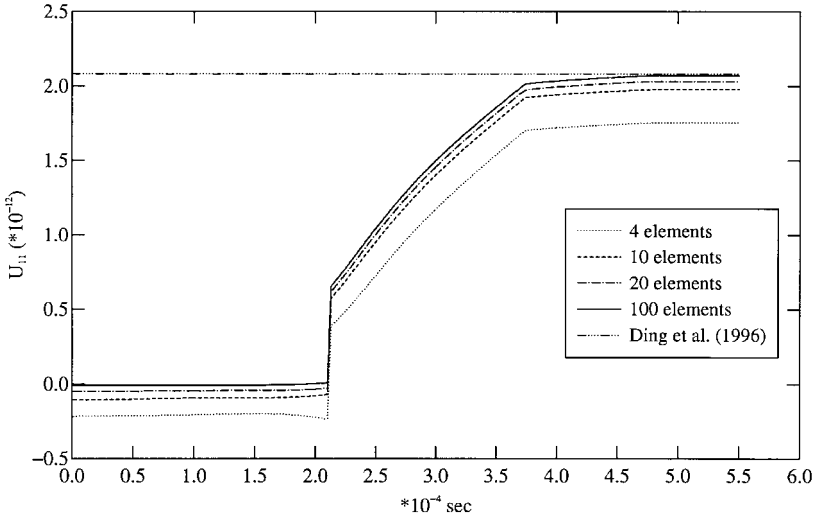


Fig. 12. $U_{II}$ for PZT-6$B$, $\mathbf{x} = (1, 0, 0)$.

Fig. 12 shows the convergence of $U_{11}(1, 0, 0, t)$ for PZT-6$B$ versus the number of quadratic elements used in the numerical integration. One can observe that the kernel $M_{11}^{**}$ demands a fine discretization to converge to the analytical static results from Ding et al. (1996).

## 9. Conclusions

The formulation from Khutoryansky and Sosa (1995a, b) was implemented in the present work rendering good numerical results for the analysed examples. The operator $\mathbf{Q}$ for the class 6 mm was factored into a product of a second and a fourth degree operators, enabling a generalization of Payton's earlier results on the Herglotz–Petrowski formulas for hexagonal materials (Payton, 1983). The presented numerical examples confirm the existence of singularities of various orders that travel on the wave front outward from the point of excitation.

## Acknowledgements

C.H. Daros thanks the DAAD (Deutscher Akademischer Austauschdienst) for the financial support.

## References

Akamatsu, K., Tanuma, K., 1997. Green's functions of anisotropic piezoelectricity. Proceedings of the Royal Society of London A 453 (1958), 473–487.

Burridge, R., 1967. The singularity on the plane lids of the wave surface of elastic media with cubic symmetry. The Quarterly Journal of Mechanics and Applied Mathematics 20, 41–56.

Chen, T., 1993. Green's functions and the non-uniform transformation problem in a piezoelectric medium. Mechanics Research Communications 20, 271–278.

Dieulesaint, E., Royer, D., 1980. Elastic Waves in Solids. John Wiley, New York.

Ding, H.J., Liang, J., Chen, B., 1996. Fundamental solutions for transversely isotropic piezoelectric media. Science in China A 39 (7), 766–775.

Duff, G.F.D., 1960. The Cauchy problem for elastic waves in an anisotropic medium. Philosophical Transactions of the Royal Society of London A 252 (31), 249–273.

Duff, G.F.D., 1977. Hyperbolic differential equations and waves. In: Garnir, H.G. (Ed.), Boundary Value Problems for Linear Evolution Partial Differential Equations. D. Reidel Publishing Co, Dordrecht, Holland, pp. 27–155.

Dunn, M., Wienecke, H., 1996. Green's functions for transversely isotropic piezoelectric solids. International Journal of Solids and Structures 33 (30), 4571–4581.

Every, A.G., McCurdy, A.K., 1987. Phonon focusing in piezoelectric crystals. Physical Review B 36 (3), 1432–1447.

Every, A.G., Neiman, V.I., 1992. Reflection of electroacoustic waves in piezoelectric solids: mode conversion into four bulk waves. Journal of Applied Physics 12 (15), 6018–6024.

Every, A.G., Kim, K.Y., 1994. Time domain dynamic response functions of elastically anisotropic solids. The Journal of the Acoustical Society of America 95, 2505–2516.

Gelfand, I.M., Shilov, G.E., 1964. Generalized Functions, vol. 1. Academic Press, New York.

John, F., 1955. Plane Waves and Spherical Means Applied to Partial Differential Equations. Interscience, New York.

Khutoryansky, N.M., Sosa, H., 1995a. Dynamic representation formulas and fundamental solutions for piezoelectricity. International Journal of Solids and Structures 32 (22), 3307–3325.

Khutoryansky, N.M., Sosa, H., 1995b. Construction of dynamic fundamental solutions for piezoelectric solids. Applied Mechanics Reviews 48 (11), 222–229.

Musgrave, M.J.P., 1996. Crystal Acoustics. Holden–Day, San Francisco.

Norris, A.N., 1994. Dynamic Green's functions in anisotropic piezoelectric, thermoelastic and poroelastic solids. Proceedings of the Royal Society of London A 447, 175–188.

Payton, R.G., 1983. Elastic Wave Propagation in Transversely Isotropic Media. Martinus Nijhoff Publishers, The Hague.

Salmon, G., 1927. A Treatise on the Analytic Geometry of Three Dimensions. Chelsea Publishing Company, New York.

Strashilov, V., Gentchev, K., 1987. Computation method for slowness curves in materials with arbitrary piezoelectricity. Acoustics Letters 11 (2), 26–30.